Biosensors and Bioelectronics 141 (2019) 111360

Contents lists available at ScienceDirect

Biosensors and Bioelectronics

journal homepage: www.elsevier.com/locate/bios

General-purpose passive wireless point–of–care platform based on smartphone

Pablo Escobedo[a,c,1], Miguel M. Erenas[b,c,1], Antonio Martínez-Olmos[a,c], Miguel A. Carvajal[a,c], Sara Gonzalez-Chocano[b], Luis Fermín Capitán-Vallvey[b,c], Alberto J. Palma[a,c,*]

[a] ECsens, CITIC-UGR, Department of Electronics and Computer Technology, University of Granada, Campus Aynadamar, 18071, Granada, Spain
[b] ECsens. Department of Analytical Chemistry. Campus Fuentenueva, Faculty of Sciences, University of Granada, 18071, Granada, Spain
[c] Unit of Excellence in Chemistry applied to Biomedicine and the Environment of the University of Granada, Granada, Spain

ARTICLE INFO

Keywords:
Passive point-of-care platform
Electrochemiluminescence
Electrochemical techniques
Smartphone
Energy harvesting
Near-field communication

ABSTRACT

A versatile, compact and low-cost analytical platform has been designed, tested and validated to be used in the point-of-care settings. This passive measurement system is powered and complemented by a standard smartphone including a programmed application for measurement configuration and data processing as well as wireless results sharing. Electrochemical and electrochemiluminescence analytical techniques can be configured and realized by this platform that employs standard screen-printed electrodes for the sample managing and off-the-shelf electronic components. The power, electrical and optical signal processing have been studied in depth. The system can harvest energy up to 22.5 mW, set up a voltage in the range of ± 1.15 V, and measure potentials in a range of 600 mV with an uncertainty of 1 mV, and current from 2 μA to 0.75 mA with a resolution of 1.1 μA. Moreover, standard tests have been performed to the platform consisting of amperometric, potentiometric, cyclic voltammetry and electrochemiluminescent analytical techniques, showing excellent agreement with a reference instrument. Finally, our design has also been applied to glucose, pH and H_2O_2 determinations, providing the full analytical parameters which are in very good agreement with the reference instrument results. Ranges (0.065–0.75 M, 0.62–100 mM and 3–9 pH units for glucose, H_2O_2 and pH, respectively) and limits of detection (0.024 M and 0.03 mM for glucose and H_2O_2, respectively) make this low-cost platform (< US$8) suitable for analytical applications.

1. Introduction

Electrochemical (EC) and electrochemiluminescence (ECL) have proved to be quantitative high resolution (bio)-analytical techniques presenting high selectivity and sensitivity (Capitán-Vallvey et al., 2018; Hesari and Ding, 2016; L. L. Li et al., 2017; Y. Y. Li et al., 2017; Paschoalino et al., 2019; Sierra et al., 2019). They are routinely used in clinical and analytical laboratories for detecting a wide diversity of analytes (e.g., proteins, nucleic acids, metabolites, metals) for personal and public health, clinical analysis, food and water quality, and environmental monitoring (Deng and Ju, 2013; Jolly et al., 2016; Magerusan et al., 2017; Mani et al., 2015; Vacek et al., 2016; Wang et al., 2017; Wu et al., 2016) in many cases as wearable devices (Anastasova et al., 2016; Bandodkar et al., 2015; Gao et al., 2016; Imani et al., 2016; Nyein et al., 2016; Panneer Selvam et al., 2016; Sempionatto et al., 2017). Undoubtedly useful in a large set of scenarios, these analytical methods (with the important exception of blood glucose personal meters (Freckmann et al., 2012)) are generally implemented in well-resourced laboratories realized by high qualified personnel with expensive and bulky equipment. A step forward in the dissemination of these analytical techniques should be to enable them to be performed and communicated in any setting. Therefore, keeping the analytical parameters (limit of detection, ranges, resolution and selectivity as the most important features) as close as possible to the laboratory instrumentation, the design of an affordable and easy-to-use platform to realize complete EC and ECL analyses is still a notable research challenge as reported in some pioneering designs (Lillehoj et al., 2013; Nemiroski et al., 2014).

In this regard, tests at the point-of-care (PoC) (Dincer et al., 2017; Min et al., 2018; Wu et al., 2017; Zarei, 2017) are an alternative approach to laboratory-based analyses that provide diagnostic information in an outpatient setting (Boppart and Richards-Kortum, 2014),

* Corresponding author. Unit of Excellence in Chemistry applied to Biomedicine and the Environment of the University of Granada, Granada, Spain.
E-mail address: ajpalma@ugr.es (A.J. Palma).
[1] Both authors have equally contributed to this work.

https://doi.org/10.1016/j.bios.2019.111360
Received 5 March 2019; Received in revised form 16 May 2019; Accepted 27 May 2019
Available online 30 May 2019
0956-5663/

thereby reducing the time and infrastructure necessary for clinical decision making (Drain et al., 2014). In resource-limited settings, PoC testing offers important clinical benefits, including reduced clinical infrastructure and fewer patients lost to follow-up. According to this, the World Health Organization (WHO) called for PoC tests to meet specific ASSURED criteria: Affordable, Sensitive, Specific, User-friendly, Rapid and robust, Equipment-free, and Deliverable to end-users (Peeling et al., 2006). Indeed, the global point-of-care diagnostics market was valued at $21.40 Billion in 2016 and is expected to reach $38.13 Billion by 2022, at an estimated compound annual growth rate (CAGR) of 10.0% from 2016 to 2022 (marketsandmarkets.com, 2018).

Smartphones can be currently considered as mini computers with high performance microprocessors and high capacity memories, high quality CMOS-based cameras and other physical sensors, multiple communication capabilities (Bluetooth, RFID, 4G, etc.), operating systems and versatile software toolkits for signal processing. Adding some accessories, they are revolutionizing the design of advanced analytical sensing systems classified as PoC systems with some applications until recently unthinkable (García et al., 2011; Guo, 2017; Ji et al., 2017; Lopez-Ruiz et al., 2014; Roda et al., 2016; Steinberg et al., 2015). These are usually cheaper than the miniaturized analytical devices, are globally widespread and easy to use for the public, which would significantly enhance the diagnostic abilities (Kanchi et al., 2018). Another research and developing field that is changing the paradigm of analytical PoC systems are those measurement platforms fully passive (i.e. extracting the required power for functioning by energy harvesting) significantly decreasing the maintenance and cost needs (Ostfeld et al., 2016; Potyrailo, 2016). With this respect and in connection with smartphone features, near-field communication (NFC) is a set of low speed and low range communication protocols included in recent smartphones that is used in contactless payment systems and social networking. It is able to wirelessly power and exchange information using a radiofrequency signal between an NFC-enabled device and an NFC passive tag or another active device. This capability to power electronic systems is being employed very recently in complex measurement platforms thanks to highly advanced power management electronic chips together with electronic designs for ultra-low power circuits (Escobedo et al., 2017; Heikenfeld et al., 2017; Steinberg et al., 2016).

Here, we present a universal and fully configurable passive analytical platform to perform EC and ECL analyses and to transmit the results of these analyses in any setting with the only support of a smartphone. Our system has been designed as an attachment consisting of printed circuit boards (PCB) together with an ambient light shielding enclosure to be coupled to a smartphone with NFC interface and image detection capabilities. Analytical techniques are configured and results are presented and shared with a user-friendly software application programmed in the smartphone. The developed electronic hardware has been optimized and fabricated with off-the-shelf electronic components, needing no additional battery. Required energy is harvested from the NFC link, which is also used for bidirectional communication with the smartphone that is employed as signal processing as well as sharing data device. In this report, the proposed platform includes a broad range of electrochemical techniques such as amperometry; different forms of voltammetry: cyclic, differential pulse, and square wave; potentiometry and electrochemiluminescence and their performance has been characterized with common electroactive models and validated with representative applications, using a commercial electrochemical analyzer as a reference instrumentation.

2. Materials and methods

2.1. PCB design and fabrication

The proposed system comprises as main electronic components an LMP91000 potentiostat chip (POT) (Texas Instruments, Dallas, Texas, USA), a low-power microcontroller unit (LPMCU) model PIC16LF1703 (Microchip Technology Inc., Chandler, Arizona, USA), an instrumentation amplifier INA321 (Texas Instruments, USA), an NFC chip AS3955 (AMS AG, Unterpremstätten, Austria), and a custom-designed RFID antenna. The LMP91000 is a miniaturized configurable analog front end (AFE) potentiostat for low-power chemical sensing applications. The platform was fabricated on FR4 substrate using a mechanical milling machine model ProtoMat S100 (LPKF Laser & Electronics AG, Garbsen, Germany). The FR4 had a thickness of 1.5 mm, a relative permittivity of $\varepsilon_r = 4.6$ and a loss tangent of $\tan\delta = 0.015$. Metallization layer was copper 35 µm thick with a conductivity of $\sigma = 4.6 \times 10^7$ S/m.

2.2. Antenna design and characterization

The mentioned NFC chip along with the antenna enables batteryless designs. This is achieved by harvesting energy from the electromagnetic field induced by an external RFID reader to supply the rest of the circuitry with a current up to 5 mA at a regulated voltage of 4.5 V. The antenna is a custom-designed planar coil. Resonance is achieved at $f_0 = 1/2\pi\sqrt{LC}$, with C = 45 pF being the integrated capacitor of the AS3955 chip at the frequency of interest, 13.56 MHz. Thus, the inductance value required for the resonance of the tag at $f_0 = 13.56$ MHz is about L = 3.06 µH. The designed antenna coil has eight turns and dimensions of 31 mm × 20 mm, being 250 µm the width of the conductor and the interspacing between the lines. The final dimensions and number of turns for the antenna were obtained after optimization process with EM simulation using Advanced Design Simulator (ADS, Keysight Technologies, Santa Clara, CA, USA). COMSOL Multiphysics (COMSOL AB, Stockholm, Sweden) was used for the numerical simulation of the coupling factor of the smartphone and our system antennas (see Supplementary Information (SI)). The frequency response of the fabricated antenna was evaluated using a Precision Impedance Analyzer 4294 A and an Impedance Probe Kit 4294A1 (Keysight Technologies, Santa Rosa, CA, USA).

2.3. Android™ application development

A user-friendly custom Android™ application was developed to use an NFC-enabled smartphone as the external reader for both communication and energy harvesting purposes. Android Studio 3.1.2 was used as the integrated development environment (IDE) to code the application. The application was designed and tested against API 26 (Android 8.0). However, it supports different Android versions as the lowest API level compatible with the application is API 18 (Android 4.3).

The application takes control of the two interfaces of the mobile phone used in this system: the NFC and the rear camera. The NFC link is used to power up the whole system and communicate with the LPMCU. In this regard, the application allows the user to configure different parameters within a finite state machine that has been coded in the LPMCU. The information is exchanged between the application and the LPMCU by means of NFC commands. The different EC and ECL reactions start when the desired potential difference is established between the electrodes, which can be controlled by the user through the Android application. In the case of ECL, the application takes control of the rear camera as soon as the user clicks on the *Start* button of the corresponding user interface. The part of the application that controls the phone camera is responsible for the acquisition and processing of the luminescent signal resulting from the ECL reactions. The algorithms developed to accomplish these acquisition and processing tasks are based on the computer vision OpenCV 3.1.0 Android library (Bradski, 2000). In the cases of potentiometry, amperometry and CV, MPAndroidChart open source charting library version 3.0.3 was used for data visualization (Jahoda, 2016). Additional information and screenshots of the Android application are shown in the Supplementary Information of

this work (Fig. S2).

2.4. Video processing for ECL

The video recorded using the smartphone is processed to measure the intensity of the captured ECL signal. This luminescence is quantified by adding the value of all the pixels in each frame. In this way, we obtain a sampled intensity signal with sampling frequency of 30 Hz, since the smartphone recording velocity is 30 frames per second. Each frame is filtered in order to reduce noise due to background light. The filtering process consists of the application of a threshold limit where all the pixels whose value is lower than a given limit are set to zero. The value of the limit is obtained from the analysis of the first ten dark frames of the video without luminescence. For these frames, the mean value of the intensity plus four times the standard deviation is taken as the limit for the threshold filter. This number was selected after a statistical analysis using MATLAB® software (MathWorks, Natick, MA, USA) where the cumulative distribution function (CDF) of the pixels in each frame is generated. From this CDF it is possible to state that more than 99.5% of the pixels in these dark images have an intensity value below the limit given by the mean value of the intensity plus four times the standard deviation. Therefore, if a threshold filter with this limit is applied, all these pixels which are considered noise are filtered.

2.5. Reagents and electrodes

Dihydrogen potassium phosphate, monohydrogen potassium phosphate, luminol, Trizma base, hydrogen peroxide, potassium chloride, potassium hexacyanoferrate(III), potassium hexacyanoferrate(II) trihydrate, aniline, hydrochloric acid and glucose oxidase. All the reagents were of analytical grade and purchased from Sigma-Aldrich (Merck KGaA). Reverse-osmosis type quality water (Milli-Q Plus185 from Millipore, Molsheim, France) was used throughout.

Commercial screen-printed electrodes (SPE) from ItalSens were purchased at PalmSens (Houten, The Netherlands). The electrochemical cell was screen-printed on a polyester support, composed by a counter and working carbon electrodes and an AgCl/Ag pseudo reference electrode. Before being used, the electrochemical cells were tested to check uniform behaviour. To prepare a receptacle on the disposable electrochemical cell, the electrode area was covered with layers of plastic white adhesive tape up to 1 mm in thickness and 8 mm diameter hole in the sensing area with an approximate volume of 50 µL.

2.6. Performance test of the smartphone-based platform

To evaluate the performance of the PoC platform for the different techniques we compared it with the commercial electrochemical workstation AUTOLAB PGSTAT302N potentiostat/galvanostat as reference instrument (Metrohm AG-Herisau, Switzerland). All measurements were performed in the disposable SPE previously described. Cyclic voltammetry was carried out by recording cyclic voltammograms to the ferrocyanide/ferricyanide redox couple at 3.4 mM in 1 M KCl by varying potentials from -0.1–0.6 V at a scan rate of 0.5 V/s. For chronoamperometry measurements, a solution of 3.4 mM ferrocyanide was used working at 0.5 V for 30 s. For potentiometry, solutions with different ferrocyanide/ferricyanide ratio were tested and the potential difference was measured after 30 s. For electrochemiluminescence, a 0.5 V potential was applied for 1 s to a solution containing 0.02 M luminol in 0.1 M NaOH and 50 mM H_2O_2 in 0.5 M TRIS buffer pH 9.0 and the luminescence signal generated was registered by a smartphone working in video mode. More details are included in SI.

2.7. Analytical procedures

The PoC platform was also applied in three different procedures to test their potential usefulness; namely amperometric determination of glucose, potentiometric determination of pH and electrochemiluminescence procedure for determination of hydrogen peroxide. Figures of merit of the analytical procedures were calculated, obtaining the limit of detection as three times the standard deviation (SD) of the blank and the precision in terms of coefficient of variation.

2.7.1. Determination of glucose

It was performed by addition on the receptacle of SPE of 20 µL of 250 U/mL glucose oxidase solution in 1.0 M KCl, 20 µL of 600 mM $K_3[Fe(CN)_6]$ and 20 µL of glucose standard between 0.01 and 0.75 M in pH 7.0 phosphate buffer. The current intensity was measured after applying 0.6 V for 60 s.

2.7.2. Determination of pH

SPE electrochemical cells are used with the working electrode coated with PANI prepared by cyclic voltammetry (see SI). The potential was measured after adding 40 µL of different pH standards 30 s after the addition of the sample, obtaining 3 replicates per sample.

2.7.3. Determination of H_2O_2

The ECL signal was recorded with the smartphone working in video mode after applying a potential of 0.5 V during 1 s to a SPE cell containing a solution prepared with 20 µL of 0.02 M luminol in 0.1 M NaOH and 20 µL of H_2O_2 standards in 0.5 M TRIS buffer pH 9.0 with 5 replicates per standard.

3. Results and discussion

3.1. System design and operation

A picture of the complete PoC platform is shown in Fig. 1(a) in operative mode. This analytical system has been designed, fabricated and tested to be able to configure and collect data from potentiometric and amperometric (bio-)sensors as well as cyclic voltammetry (CV) and electrochemiluminescence (ECL) analytical techniques with the same electrode interface. System is powered by a standard smartphone where a custom-developed application sets up the analytical procedure, configures the optical and electrical signal interface, processes the data, and shares the results. Moreover, optical ECL signal is captured by the smartphone built-in video camera. Therefore, our platform is capable to implement four analytical measurement procedures including electrical and optical (bio-)analytical techniques that can be compatible on standard two or three electrochemical electrodes for *in situ* measurement with a user-friendly interface. Fig. 1(b) displays separately the three main parts of the system: 1) printed board circuits (PCBs) for signals processing/transmission and power management with the SPE attached, 2) the smartphone with the application running and 3) a black methacrylate-made accessory to hold both former parts with the double aim of system alignment and ambient light shielding. As shown in Fig. 1(c), the PCB design has been split into two different PCBs interconnected by a vertical connector: i) the PCB1 containing a planar inductor and the RFID/NFC chip for RF power harvesting and data communication from/to the smartphone NFC reader, and ii) the PCB2 for SPE interfacing, data processing and additional power management controlled by the low-power microcontroller (LPMCU). PCBs were designed and fabricated separately because the NFC antenna reader can be located in different positions depending on the smartphone, therefore the PCB1 can be redesigned according to this fact without changing the main PCB2. Moreover, both PCBs were fabricated in vertically-shifted planes, on the one hand to allow the closest contact between smartphone and PCB antennas to maximize energy transfer and improve data communication and, on the other hand, to move the electrode away from the smartphone camera for a suitable image capture required in the ECL technique. PCBs picture is shown in Fig. 1(d).

Fig. 1(e) illustrates the schematic, power and data flow of the PCBs. For low power operation, NFC chip was programmed to provide a

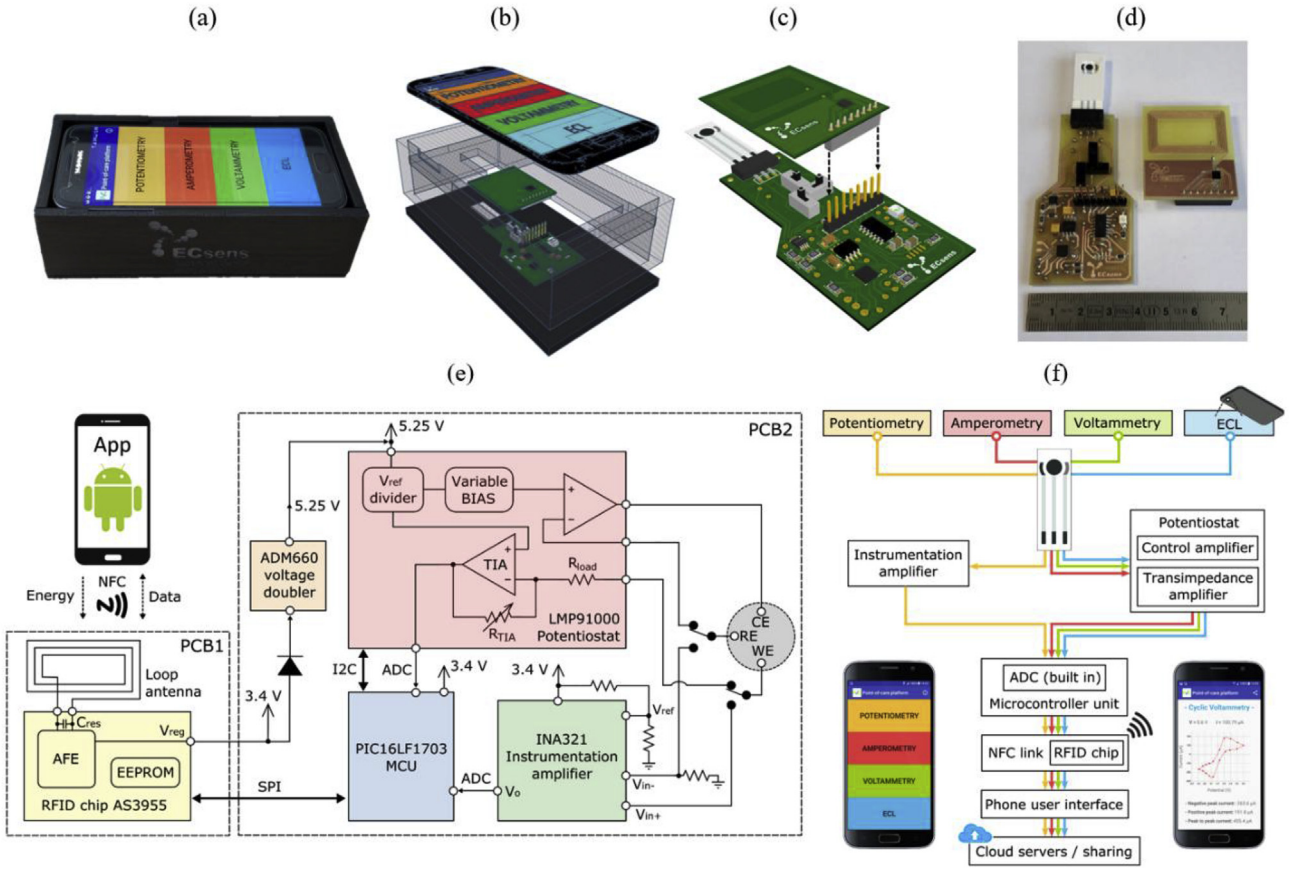

Fig. 1. Images and schematic illustrations of the smartphone-based analytical PoC platform. (a) Picture of the complete PoC platform in operative mode showing the black methacrylate holder accessory as the ambient light shielding enclosure to accommodate the PCBs and the NFC-enabled mobile phone running the custom-developed application. **(b)** Rendered exploded view of the complete PoC platform with a see-through view of the holder accessory to show the positioning and alignment of the PCBs inside it. **(c)** Rendered 3D detailed view of the designed PCBs for signal processing/transmission and power management. **(d)** Photograph of the fabricated PCBs with the SPE attached. **(e)** Schematic, power and data flow of the PCBs for power management (PCB1) and signals processing/transmission (PCB2) showing all the components involved in the operation. **(f)** System-level block diagram of the PoC platform showing the signal transduction, conditioning, processing and wireless transmission paths from the electrode to the custom-developed mobile application for amperometry, potentiometry, cyclic voltammetry and electrochemiluminescence techniques. The inset images show the home page (left) and the real-time data display page for cyclic voltammetry (right) of the mobile application.

regulated voltage of 3.4 V from the RF energy harvested by the antenna to directly power the LPMCU and the instrumentation amplifier (INA). This voltage is boosted to 5.25 V by a switched-capacitor voltage converter to power and to span the output voltage capabilities of the potentiostat chip (POT) LMP91000. On the other hand, POT is configured by LPMCU with a serial inter-integrated circuit (I2C) bus and analog signals coming from sensors through POT and INA are converted to digital and averaged (low pass filter function) in the LPMCU to enhance the signal-to-noise ratio. Smartphone custom-developed application takes control of the whole measurement process sending/receiving information from the NFC chip that communicates with the LPMCU by means of a serial peripheral interface (SPI) bus. Shown switches are included to select the required connections for each technique. The system operation is also depicted in Fig. 1(e) where INA amplifies the output voltage of the potentiometric sensor whereas POT biases the 3-terminal electrode to implement amperometry, CV and ECL techniques and conditions the output current coming from CV and amperometric measurements. ECL signal is collected by the smartphone camera configured as video camera and processed as explained below. LPMCU computational and interface capabilities are used for signal pre-processing and communication to the smartphone through the NFC chip. Fig. 1(f) shows the system-level block diagram of the platform showing the signal transduction, conditioning, processing and wireless transmission paths from the electrode to the custom-developed mobile application for the different techniques.

A cost breakdown of the proposed platform is provided in SI, resulting in around US$7.69 under mass production. It is expected that the cost of the PCB manufacturing would be only a small percentage of the total components cost under mass production. Therefore, the developed system is on the same line or even cheaper in terms of cost-effectivity than other low-cost smartphone-based PoC platforms that can be found in the literature (Fan et al., 2017; Muñoz-Berbel et al., 2018; Nemiroski et al., 2014; Wang et al., 2015).

Detailed configuration procedures and signal processing algorithms will be explained below in the subsections devoted to each of the implemented analytical techniques.

3.2. Power, electrical and optical signals processing

One of the keys of the design relays on an efficient energy harvesting to provide enough power not only for the electronic components but also for the electrochemical reactions occurring in the electrode. The chosen NFC chip is able to provide up to 5 mA at 4.5 V (i.e. 22.5 mW) in optimal energy harvesting conditions. This can be achieved with an optimized coil design of the PCB1 together with an aligned and close positioning related to the coil of the smartphone NFC. A planar rectangular loop antenna was designed for this application due to its planar design and efficient area utilization. External dimensions

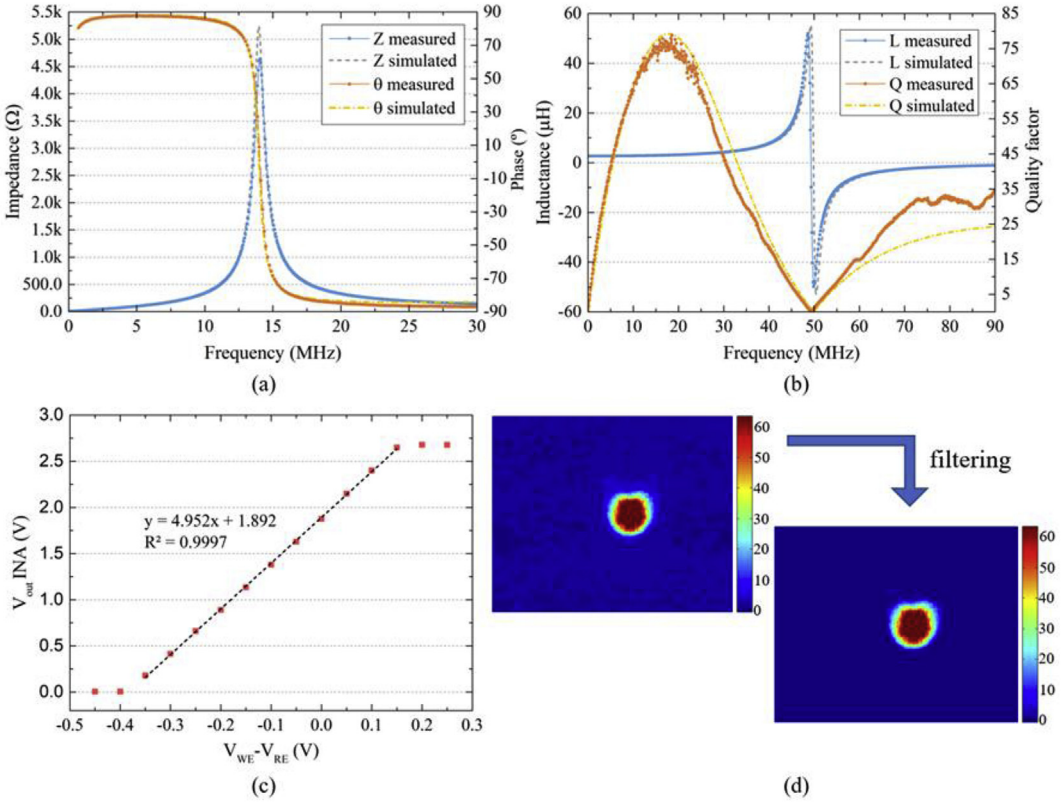

Fig. 2. Power, electrical and optical signals characterization and processing. (a) Simulated and measured frequency response of the inductance (L) and quality factor (Q) of the designed coupling coil. **(b)** Simulated and measured frequency response of the impedance (Z) and phase (θ) of the complete LC resonator that comprises the NFC antenna ensuring efficient RF energy transfer from the smartphone to the rest of electronics. **(c)** Experimental characterization of the micropower INA as a function of the potential between working and reference electrodes. **(d)** Example of original frame showing the cumulative distribution function (CDF) of the pixels of an optical ECL recorded signal, and the same frame after applying a filtering process to reduce noise due to background light. The color scale depicts the value of the intensities computed as the sum of the value of all the pixels within the frame. (For interpretation of the references to color in this figure legend, the reader is referred to the Web version of this article.)

and turn interspace were constrained by NFC reader dimensions and PCB drilling machine resolution respectively. Number of turns and line width were calculated to achieve a resonance frequency of 13.56 MHz together with the chip internal capacitor. For design optimization purposes, ADS simulator was used to account for the effect of the environment (smartphone and PCB substrate) on the antenna performance. Fig. 2(a) shows the good agreement between the numerical simulation and experimental inductance, L, and quality factor, Q, of the coupling coil with experimental values of L = 2.85 μH, Q = 73 at 13.56 MHz. Fig. 2(b) depicts the comparison of numerical and experimental data for the complete LC resonator of the PCB1 showing excellent matching and ensuring an efficient RF energy transfer from smartphone to PCBs. Maximum distance between smartphone and PCB1 coils for working system was 8.4 mm. COMSOL simulation of the coupling factor of this system (modelled as a transformer with air core) as a function of the distance pointed out that this parameter is critical, requiring more than 93% of maximum coupling to power up our system (simulation results are given in Figs. S1(a) and S1(b) in the SI). PCB2 powering with 3.4 V from NFC chip was stable and uninterrupted up to 200 s with a voltage standard deviation of 2.5 mV_{rms} (< 800 ppm) that is enough for the analytical procedures.

Regarding the electrical characterization of PCB2 components and accounting for the 10 bits LPMCU analog-to-digital converter (ADC), experimental INA signal-to-noise ratio (SNR) was 60 dB with an excellent linearity as shown in Fig. 2(c). This micropower INA has been layout with active guard around its input signal tracks to preserve its low input current and high input resistance (10^{13} Ω) for stable and accurate potentiometry measurements. Configured with the recommended gain of 5 V/V, differential input voltage swing was 600 mV covering ten decades of the ideal Nernst equation. Moreover, the input-referred minimum differential voltage able to be measured was 1 mV. Experimental INA power consumption was 0.2 mW. Experimentally determined POT specifications relevant to CV and ECL techniques were (see more information in Figs. S1(c) and S1(d) in SI): i) full scale output voltage bias: ± (1.159 ± 0.003) V, ii) Slew rate in pulse mode: (0.0140 ± 0.008) V/μs, iii) repeatability in pulse mode bias calculated as standard deviation of ten 0.5 V pulses of 1 s and separated 3 s was 1.3 mV_{rms}, and iv) average maximum sweep voltage in triangular mode at full output span: 0.48 V/s. Its built-in transimpedance amplifier was configured to provide a current span from 2 μA to 0.75 mA with a resolution of 1.1 μA as it was experimentally tested. Measured maximum power consumptions were 0.53 mW and 5.8 mW for POT and LPMCU respectively.

With the video processing detailed above, in Fig. 2(d) the difference between an original and filtered frame can be observed. From these filtered frames the intensity is obtained as the sum of the value of all the pixels. A normalization process is carried out in order to take into account the area of the electrode in which the luminescence is produced. This effective area varies from one electrode to other, which causes a decrease in the repeatability of the measurements. The normalization consists of the calculus of the ratio between intensity and number of non-zero pixels, which provides the intensity per pixel for each frame, named as normalized optical intensity, NOI. This parameter has proven to present a lower dispersion for different replicas of the same measurement.

After this processing, the luminescence recorded in the video is shown as a normalized intensity signal as Fig. 3(d) depicts. Several features can be extracted from this signal to find a relationship between

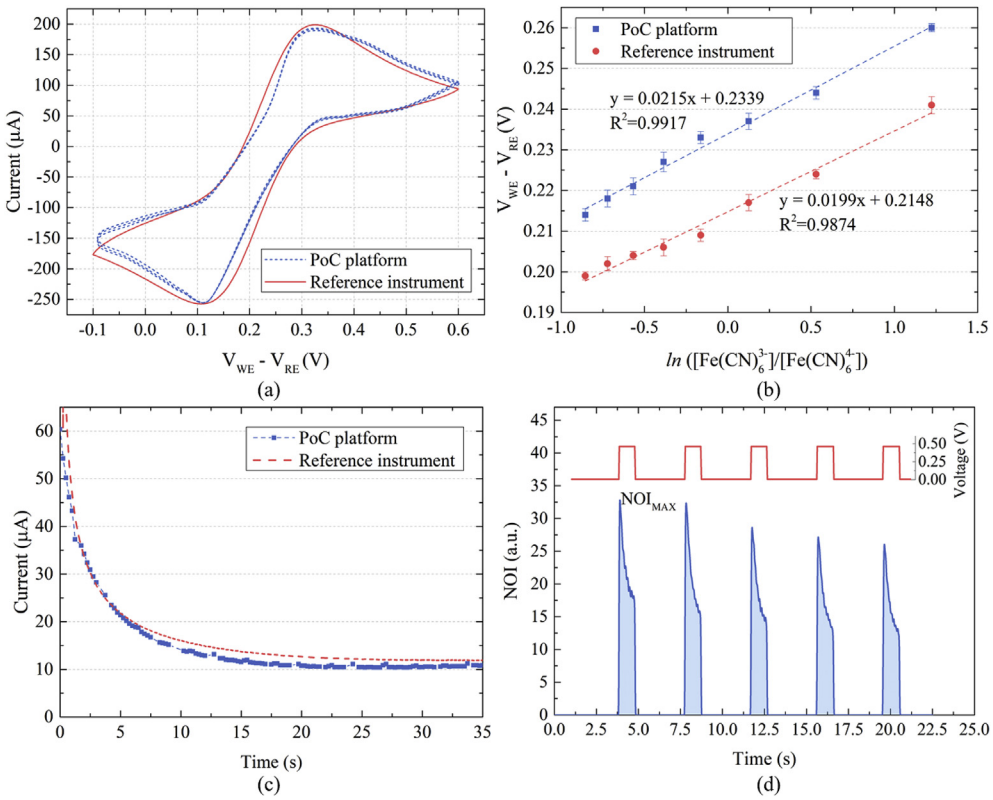

Fig. 3. PoC platform validation. Comparison between signals acquired by the described platform and a commercial electrochemical instrument using ferricyanide/ferrocyanide couple for **(a)** cyclic voltammetry, **(b)** potentiometry and **(c)** chronoamperometry. In case of ECL **(d)**, the well-known system luminol – H_2O_2 has been used as a model. Graph **(d)** represents the normalized optical intensity, NOI, obtained from the filtered frames as the sum of the value of all the pixels when 0.5 V pulse voltages are applied. NOI_{MAX} is also shown as the maximum at the first voltage pulse.

the temporal evolution of the luminescence and the concentration of the analyte under study. After testing different parameters, the analytical parameter considered in this work was the maximum value reached by the normalized optical intensity in the first applied pulse, NOI_{MAX}.

3.3. Performance of the PoC platform

The comparison between signals acquired by the described platform and a reference electrochemical workstation using the same electrochemical cells and solutions is presented in Fig. 3 for the different electrochemical techniques included in the platform. Experiments with ferricyanide/ferrocyanide redox couple were conducted to test the performance of the system in the measurement of potentials and currents. Fig. 3(a) displays the cyclic voltammograms of the redox couple at a SPE cell (for more information see SI), showing a cathodic peak at 0.12 V with a current of 300 μA for both instruments, and an anodic peak at 0.33 V with a current of 227 μA for the workstation and 239 μA for the platform. In the case of potentiometry, the evolution of potential with ln([ferricyanide]/[ferrocyanide]) ratio is compared for the platform and the workstation in Fig. 3(b), presenting similar slopes (P-value 0.195). Chronoamperometric measurements are available with this platform as Fig. 3(c) shows using ferrocyanide as a model. Regarding ECL, we have used the well-known system luminol-H_2O_2 as a model using a set of consecutive pulses of 1 s at 0.5 V each 10 s (Fig. 3(d)).

The PoC platform reliability is assessed with the very good agreement shown between the reference instrumentation and our PoC test results.

3.4. Applications of the PoC platform

The developed platform has been applied and evaluated for the determination of some common analytes. The analytical parameters of the methods are showed and compared to the reference instrumentation in Table 1.

3.4.1. Determination of glucose by chronoamperometry

Glucose determination is based on the chronoamperometric measurement of ferrocyanide resulting from enzymatic oxidation of glucose and concomitant reduction of ferricyanide. The procedure was applied to platform and reference instrument using the same solutions, obtaining calibration functions adjusted to a sigmoid by the Boltzmann equation (Fig. 4(a)). A limit of detection of 0.024 M and range from 0.065 M to 0.750 M was obtained with this platform compared to a detection limit of 0.038 M of and range from 0.073 M to 0.750 M for the electrochemical workstation. In both instruments, the precision is around 16%. Correlation curves of the currents obtained by reference instrument and platform are presented in the SI (Fig. S5).

3.4.2. pH measurement by potentiometry

pH is measured using a PANI coated SPE electrode. Fig. 4(b) shows the calibrations using both the proposed and the reference instruments with very similar results in terms of slope (-0.056 V and -0.059 V for reference and platform, respectively; P-value 0.513) and intercept (0.23 and 0.27 for reference and platform, respectively; P-value 0.305), with a precision of 6% and 3%, respectively (Table 1). The slope of calibration is close to the theoretical value and the correlation graph between the potential difference obtained with the reference workstation and the developed platform (Fig. S6) give a slope of 1.063 and 0.018 intercept.

3.4.3. Determination of H_2O_2 by ECL

H_2O_2 was measured based on the luminescence generated in presence of luminol when a potential difference is applied. Fig. 4(c) shows the calibration of H_2O_2 using the reference instrument and the platform recording the emission with a smartphone and considering the maximum of the normalized optical intensity, NOI_{MAX}, of the first voltage pulse as stated in the methodology Section. In both cases the exponential calibration curves are very similar (ranges from 0.47 to 100 mM and from 0.62 to 100 mM for reference instrument and platform, respectively). The obtained limits of detection were 0.04 mM and

Table 1
Analytical parameters of the methods performed with the reference instrument and the developed platform.

Determination of glucose by chronoamperometry			pH measurement by potentiometry			Determination of H_2O_2 by ECL		
$y = \frac{A_1 - A_2}{1 + e^{\frac{x - A_3}{A_4}}} + A_2$			$y = a + bx$			$y = ax^b$		
Parameter	Reference	Platform	Parameter	Reference	Platform	Parameter	Reference	Platform
A_1	-8 ± 13	-9 ± 9	a	-0.056 ± 0.004	-0.059 ± 0.004	a	21.0 ± 0.9	14.9 ± 0.5
A_2	19 ± 2	18.7 ± 0.9	b	0.23 ± 0.02	0.27 ± 0.03	b	0.12 ± 0.02	0.137 ± 0.009
A_3	0.1 ± 0.1	0.09 ± 0.09						
A_4	0.15 ± 0.07	0.12 ± 0.04						
Precision	16%	16%	Precision	6%	3%	Precision	11%	8%
Limit of detection (3·SD)	0.038 M	0.024 M				Limit of detection (3·SD)	0.04 mM	0.03 mM
Range	0.073 – 0.750 M	0.065–0.750 M	Range	3–9	3–9	Range	0.47–100 mM	0.62–100 mM
R^2	0.9818	0.9898	R^2	0.9799	0.9779	R^2	0.9999	0.9999

0.03 mM, respectively (see Table 1).

4. Conclusions

We have demonstrated a cost-effective electronic platform which, together with a smartphone, enables the implementation of the most common electrochemical and electrochemiluminescence analytical techniques. This wireless and battery-free compact system provides a low-cost (~US$8), handheld PoC platform that allows sensitive and quantitative analysis of voltammetry, potentiometry, amperometry and ECL for *in situ* and real-time applications, thus eliminating the need of expensive and bulky laboratory equipment. Moreover, the full duplex communication with the smartphone allows an easy and full reconfiguration of the experimental conditions to adapt voltage levels and waveform to the analyte under study. The operating procedure is extremely easy and training can be kept to the minimum: all that is required is to insert the screen-printed electrode, place the system in the box, apply the sample, seat the smartphone, select and configure the test, and click the play button on the screen. Just sending the analysis results, remote expertise is enabled, which is suitable to home health care or resource-limited settings. The developed system has been validated by the determination of pH, glucose and H_2O_2, obtaining technical specifications in terms of precision, limit of detection and ranges comparable to those from reference instruments.

The double alignment between both antennas for optimal energy and communication coupling and between the smartphone video camera and the strip is a design constrain that has to be carefully taken into account. In future work, we aim to improve the Android app including interactive information on optimal required alignments. In addition, double result verification can be achieved from video data and amperometric POT data for ECL techniques using simultaneously both platform capabilities.

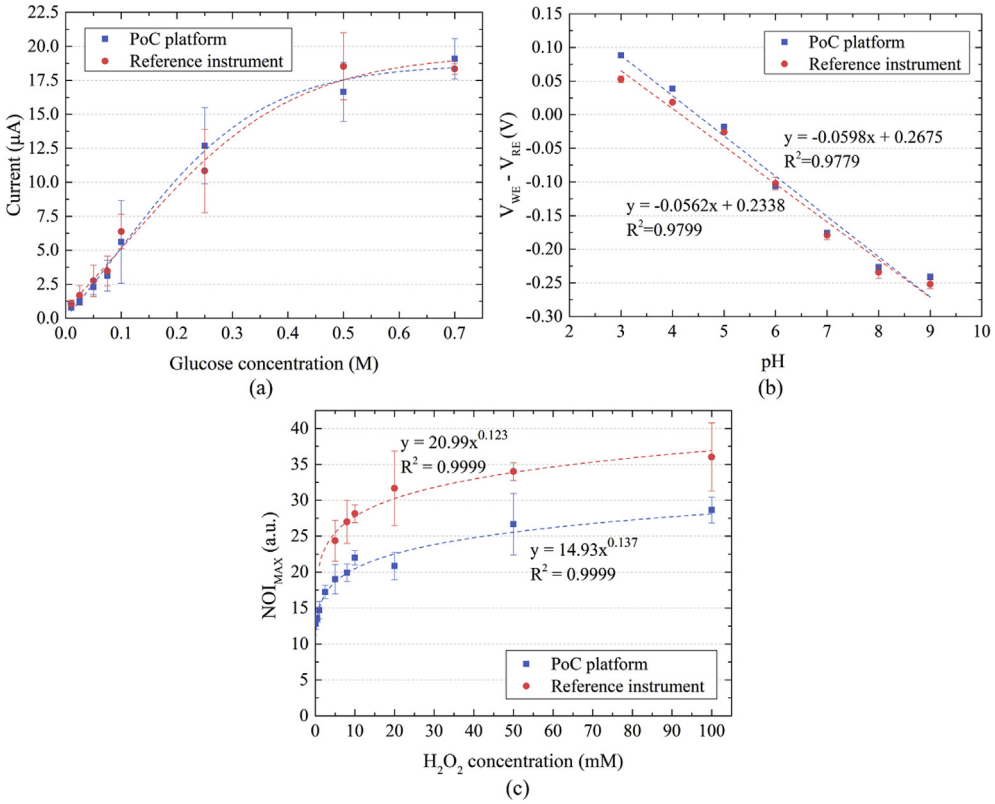

Fig. 4. PoC platform applications. Comparison between signals acquired by the described platform and the reference electrochemical instrument for: **(a)** Determination of glucose by chronoamperometry; **(b)** pH measurement by potentiometry; and **(c)** Determination of H_2O_2 by ECL.

Declaration of interests

The authors declare that they have no known competing financial interests or personal relationships that could have appeared to influence the work reported in this paper.

CRediT authorship contribution statement

Pablo Escobedo: Data curation, Investigation, Methodology, Software, Writing - original draft. **Miguel M. Erenas:** Data curation, Investigation, Methodology, Writing - original draft. **Antonio Martínez-Olmos:** Conceptualization, Data curation, Formal analysis. **Miguel A. Carvajal:** Conceptualization, Data curation, Formal analysis, Methodology. **Sara Gonzalez-Chocano:** Methodology, Resources. **Luis Fermín Capitán-Vallvey:** Conceptualization, Funding acquisition, Investigation, Methodology, Supervision. **Alberto J. Palma:** Conceptualization, Funding acquisition, Investigation, Methodology, Supervision.

Acknowledgements

This study was supported by projects from the Spanish MINECO (CTQ2016-78754-C2-1-R). The project was partially supported by European Regional Development Funds (ERDF). P. Escobedo wants to thank to the Spanish Ministry of Education, Culture and Sport for a R&D predoctoral grant (FPU13/05032).

Appendix A. Supplementary data

Supplementary data to this article can be found online at https://doi.org/10.1016/j.bios.2019.111360.

References

marketsandmarketscom, 2018. Point-of-Care/Rapid Diagnostics Market by Testing, Platform, Mode & End User - 2022. (MarketsandMarkets [WWW Document]).

Anastasova, S., Crewther, B., Bembnowicz, P., Curto, V., Ip, H.M., Rosa, B., Zhong-Yang, G., 2016. A Wearable Multisensing Patch for Continuous Sweat Monitoring. Biosens. Bioelectron. https://doi.org/10.1016/j.bios.2016.09.038.

Bandodkar, A.J., Jia, W.Z., Yardimci, C., Wang, X., Ramirez, J., Wang, J., 2015. Tattoo-based noninvasive glucose monitoring: a proof-of-concept study. Anal. Chem. 87, 394–398.

Boppart, S., Richards-Kortum, R., 2014. Point-of-care and point-of-procedure optical imaging technologies for primary care and global health. Sci. Transl. 6.

Bradski, G., 2000. The OpenCV library. Dr. Dobb's J. Softw. Tools.

Capitán-Vallvey, L.F., Palma, A.J., Olmos, A.M., Erenas, M.M., 2018. Luminescence: solid phase. In: Reference Module in Chemistry, Molecular Sciences and Chemical Engineering. Elsevier, pp. 490–520. https://doi.org/10.1016/B978-0-12-409547-2.00308-5.

Deng, S., Ju, H., 2013. Electrogenerated chemiluminescence of nanomaterials for bioanalysis. Anal. (Cambridge, United Kingdom) 138, 43–61.

Dincer, C., Bruch, R., Kling, A., Dittrich, P.S., Urban, G.A., 2017. Multiplexed point-of-care testing – xPOCT. Trends Biotechnol. 35, 728–742. https://doi.org/10.1016/j.tibtech.2017.03.013.

Drain, P.K., Hyle, E.P., Noubary, F., Freedberg, K.A., Wilson, D., Bishai, W.R., Rodriguez, W., Bassett, I.V., 2014. Diagnostic point-of-care tests in resource-limited settings. Lancet Infect. Dis. 14, 239–249. https://doi.org/10.1016/S1473-3099(13)70250-0.

Escobedo, P., Erenas, M.M., Lopez Ruiz, N., Carvajal, M.A., González Chocano, S., de Orbe-Payá, I., Capitan-Vallvey, L.F., Palma, A.J., Martínez Olmos, A., 2017. Flexible passive nfc tag for multi-gas sensing. Anal. Chem. acs.analchem 6b03901. https://doi.org/10.1021/acs.analchem.6b03901.

Fan, Y., Liu, J., Wang, Y., Luo, J., Xu, H., Xu, S., Cai, X., 2017. A wireless point-of-care testing system for the detection of neuron-specific enolase with microfluidic paper-based analytical devices. Biosens. Bioelectron. 95, 60–66. https://doi.org/10.1016/j.bios.2017.04.003.

Freckmann, G., Schmid, C., Baumstark, A., Pleus, S., Link, M., Haug, C., 2012. System accuracy evaluation of 43 blood glucose monitoring systems for self-monitoring of blood glucose according to DIN en ISO 15197. J. Diabetes Sci. Technol. 6, 1060–1075. https://doi.org/10.1177/193229681200600510.

Gao, W., Emaminejad, S., Nyein, H.Y.Y., Challa, S., Chen, K., Peck, A., Fahad, H.M., Ota, H., Shiraki, H., Kiriya, D., Lien, D.-H., Brooks, G.A., Davis, R.W., Javey, A., 2016. Fully integrated wearable sensor arrays for multiplexed in situ perspiration analysis. Nature 529, 509–514. https://doi.org/10.1038/nature16521.

García, A., Erenas, M.M., Marinetto, E.D., Abad, C.A., de Orbe-Paya, I., Palma, A.J., Capitán-Vallvey, L.F., 2011. Mobile phone platform as portable chemical analyzer. Sensor. Actuator. B Chem. 156, 350–359. https://doi.org/10.1016/j.snb.2011.04.045.

Guo, J., 2017. Smartphone-powered electrochemical dongle for point-of-care monitoring of blood β-ketone. Anal. Chem. 89, 8609–8613. https://doi.org/10.1021/acs.analchem.7b02531.

Heikenfeld, J., Jajack, A., Rogers, J., Gutruf, P., Tian, L., Pan, T., Li, R., Khine, M., Kim, J., Wang, J., Kim, J., 2017. Wearable sensors: modalities, challenges, and prospects. Lab Chip 18. https://doi.org/10.1039/C7LC00914C.

Hesari, M., Ding, Z., 2016. Review—electrogenerated chemiluminescence: light years ahead. J. Electrochem. Soc. 163, H3116–H3131. https://doi.org/10.1149/2.0161604jes.

Imani, S., Bandodkar, A.J., Mohan, A.M.V., Kumar, R., Yu, S., Wang, J., Mercier, P.P., 2016. A wearable chemical–electrophysiological hybrid biosensing system for real-time health and fitness monitoring. Nat. Commun. 7, 11650. https://doi.org/10.1038/ncomms11650.

Jahoda, P., 2016. MPAndroidChart: A powerful & easy to use chart library for Android [WWW Document]. URL. https://github.com/PhilJay/MPAndroidChart.

Ji, D., Liu, L., Li, S., Chen, C., Lu, Y., Wu, J., Liu, Q., 2017. Smartphone-based cyclic voltammetry system with graphene modified screen printed electrodes for glucose detection. Biosens. Bioelectron. 98, 449–456. https://doi.org/10.1016/j.bios.2017.07.027.

Jolly, P., Batistuti, M.R., Miodek, A., Zhurauski, P., Mulato, M., Lindsay, M.A., Estrela, P., 2016. Highly sensitive dual mode electrochemical platform for microRNA detection. Sci. Rep. 6, 1–10. https://doi.org/10.1038/srep36719.

Kanchi, S., Sabela, M.I., Mdluli, P.S., Inamuddin Bisetty, K., 2018. Smartphone based bioanalytical and diagnosis applications: a review. Biosens. Bioelectron. 102, 136–149. https://doi.org/10.1016/j.bios.2017.11.021.

Li, L., Chen, Y., Zhu, J.J., 2017. Recent advances in electrochemiluminescence analysis. Anal. Chem. 89, 358–371. https://doi.org/10.1021/acs.analchem.6b04675.

Li, Y., Li, Yuqin, Wu, Y., Lu, F., Chen, Y., Gao, W., 2017. An electrochemiluminescence biosensor for endonuclease EcoRI detection. Biosens. Bioelectron. 89, 585–591. https://doi.org/10.1016/j.bios.2016.01.082.

Lillehoj, P.B., Huang, M.-C., Truong, N., Ho, C.-M., 2013. Rapid electrochemical detection on a mobile phone. Lab Chip 13, 2950. https://doi.org/10.1039/c3lc50306b.

Lopez-Ruiz, N., Curto, V.F., Erenas, M.M., Benito-Lopez, F., Diamond, D., Palma, A.J., Capitan-Vallvey, L.F., 2014. Smartphone-based simultaneous pH and nitrite colorimetric determination for paper microfluidic devices. Anal. Chem. 86. https://doi.org/10.1021/ac5019205.

Magerusan, L., Socaci, C., Coros, M., Pogacean, F., 2017. Electrochemical platform based on nitrogen- doped graphene/chitosan nanocomposite for selective Pb 2 + detection. Nanotechnology 28, 114001.

Mani, V., Devasenathipathy, R., Chen, S.M., Vasantha, V.S., Ajmal Ali, M., Huang, S.T., Al-Hemaid, F.M.A., 2015. A simple electrochemical platform based on pectin stabilized gold nanoparticles for picomolar detection of biologically toxic amitrole. Analyst 140, 5764–5771. https://doi.org/10.1039/c5an00930h.

Min, J., Nothing, M., Coble, B., Zheng, H., Park, J., Im, H., Weber, G.F., Castro, C.M., Swirski, F.K., Weissleder, R., Lee, H., 2018. Integrated biosensor for Rapid and point-of-care sepsis diagnosis. ACS Nano 12, 3378–3384. https://doi.org/10.1021/acsnano.7b08965.

Muñoz-Berbel, X., Dei, M., Domínguez, C., Jiménez, C., Aymerich, J., Terés, L., Serra-Graells, F., Márquez, A., 2018. Cost-effective smartphone-based reconfigurable electrochemical instrument for alcohol determination in whole blood samples. Biosens. Bioelectron. 117, 736–742. https://doi.org/10.1016/j.bios.2018.06.044.

Nemiroski, A., Christodouleas, D.C., Hennek, J.W., Kumar, A.A., Maxwell, E.J., Fernandez-Abedul, M.T., Whitesides, G.M., 2014. Universal mobile electrochemical detector designed for use in resource-limited applications. Proc. Natl. Acad. Sci. Unit. States Am. 111, 11984–11989. https://doi.org/10.1073/pnas.1405679111.

Nyein, H.Y.Y., Gao, W., Shahpar, Z., Emaminejad, S., Challa, S., Chen, K., Fahad, H.M., Tai, L.-C., Ota, H., Davis, R.W., Javey, A., 2016. A wearable electrochemical platform for noninvasive simultaneous monitoring of Ca^{2+} and pH. ACS Nano 10, 7216–7224. https://doi.org/10.1021/acsnano.6b04005.

Ostfeld, A.E., Gaikwad, A.M., Khan, Y., Arias, A.C., 2016. High-performance flexible energy storage and harvesting system for wearable electronics. Sci. Rep. 6, 26122. https://doi.org/10.1038/srep26122.

Panneer Selvam, A., Muthukumar, S., Kamakoti, V., Prasad, S., 2016. A wearable biochemical sensor for monitoring alcohol consumption lifestyle through Ethyl glucuronide (EtG) detection in human sweat. Sci. Rep. 6, 1–11. https://doi.org/10.1038/srep23111.

Paschoalino, W.J., Kogikoski, S., Barragan, J.T.C., Giarola, J.F., Cantelli, L., Rabelo, T.M., Pessanha, T.M., Kubota, L.T., 2019. Emerging considerations for the future development of electrochemical paper-based analytical devices. ChemElectroChem 6, 10–30. https://doi.org/10.1002/celc.201800677.

Peeling, R.W., Holmes, K.K., Mabey, D., Ronald, A., 2006. Rapid tests for sexually transmitted infections (STIs): the way forward. Sex. Transm. Infect. 82, v1–v6. https://doi.org/10.1136/sti.2006.024265.

Potyrailo, R.A., 2016. Multivariable sensors for ubiquitous monitoring of gases in the era of internet of things and industrial internet. Chem. Rev. 116, 11877–11923. https://doi.org/10.1021/acs.chemrev.6b00187.

Roda, A., Michelini, E., Zangheri, M., Di Fusco, M., Calabria, D., Simoni, P., 2016. Smartphone-based biosensors: a critical review and perspectives. TrAC Trends Anal. Chem. (Reference Ed.) 79, 317–325. https://doi.org/10.1016/j.trac.2015.10.019.

Sempionatto, J.R., Nakagawa, T., Pavinatto, A., Mensah, S.T., Imani, S., Mercier, P., Wang, J., 2017. Eyeglasses based wireless electrolyte and metabolite sensor platform. Lab Chip 17, 1834–1842. https://doi.org/10.1039/C7LC00192D.

Sierra, T., Crevillen, A.G., Escarpa, A., 2019. Electrochemical detection based on nanomaterials in CE and microfluidic systems. Electrophoresis 40, 113–123. https://doi.

org/10.1002/elps.201800281.
Steinberg, M.D., Kassal, P., Kerekovic, I., Steinberg, I.M., 2015. A wireless potentiostat for mobile chemical sensing and biosensing. Talanta 143, 178–183.
Steinberg, M.D., Kassal, P., Steinberg, I.M., 2016. System Architectures in wearable electrochemical sensors. Electroanalysis 28, 1149–1169. https://doi.org/10.1002/elan.201600094.
Vacek, J., Zatloukalova, M., Geleticova, J., Kubala, M., Modriansky, M., Fekete, L., Masek, J., Hubatka, F., Turanek, J., 2016. Electrochemical platform for the detection of transmembrane proteins reconstituted into liposomes. Anal. Chem. 88, 4548–4556. https://doi.org/10.1021/acs.analchem.6b00618.
Wang, X., Gartia, M.R., Jiang, J., Chang, T.-W., Qian, J., Liu, Y., Liu, X., Liu, G.L., 2015. Audio jack based miniaturized mobile phone electrochemical sensing platform. Sensor. Actuator. B Chem. 209, 677–685. https://doi.org/10.1016/j.snb.2014.12.017.
Wang, X., Gao, D., Li, M., Li, H., Li, C., Wu, X., Yang, B., 2017. CVD graphene as an electrochemical sensing platform for simultaneous detection of biomolecules. Sci. Rep. 7, 1–9. https://doi.org/10.1038/s41598-017-07646-2.
Wu, W., Xiao, H., Luo, S., Liu, C., Tang, Y., Yang, L., 2016. A highly stable and effective electrochemiluminescence platform of copper oxide nanowires coupled with graphene for ultrasensitive detection of pentachlorophenol. Sensor. Actuator. B Chem. 222, 747–754. https://doi.org/10.1016/j.snb.2015.09.001.
Wu, M.Y.-C., Hsu, M.-Y., Chen, S.-J., Hwang, D.-K., Yen, T.-H., Cheng, C.-M., 2017. Point-of-Care detection devices for food safety monitoring: proactive disease prevention. Trends Biotechnol. 35, 1–13. https://doi.org/10.1016/j.tibtech.2016.12.005.
Zarei, M., 2017. Portable biosensing devices for point-of-care diagnostics: recent developments and applications. TrAC Trends Anal. Chem. (Reference Ed.) 91, 26–41. https://doi.org/10.1016/j.trac.2017.04.001.